Available online at www.sciencedirect.com

ScienceDirect

Ceramics International 40 (2014) 4491–4498

CERAMICS INTERNATIONAL

www.elsevier.com/locate/ceramint

IBLC effect leading to colossal dielectric constant in layered structured Eu_2CuO_4 ceramic

Paresh Salame, Renangso Drai, Om Prakash, A.R. Kulkarni*

Department of Metallurgical Engineering and Materials Science, IIT Bombay, Powai, Mumbai 400076, India

Received 17 July 2013; received in revised form 16 August 2013; accepted 28 August 2013
Available online 5 September 2013

Abstract

Dielectric (ε_r') studies of phase pure T′-type Eu_2CuO_4 ceramics of two markedly different grain sizes (D), prepared by (i) conventional powder mixing and (ii) citrate complexation-Pechini process, have been carried out in the frequency range 0.1 Hz to 1 MHz, and at temperatures −100 °C to 150 °C. ε_r' is found to be highly grain size dependent. For the sample with coarse bar-like grains ($D^2 \sim 17 \times 6\ \mu m^2$) ε_r' is $> 10^3$, and for the finer grain size sample with bimodal distribution ($D_1 \sim 1\ \mu m$, $D_2 \sim 3\ \mu m$) ε_r' is $\sim 10^5$; for both the samples, high ε_r' value is nearly frequency independent over 500 Hz $\leq f <$ 100 kHz and $T \geq 30$ °C. The impedance spectroscopy (IS) study has clearly shown that both, the coarse- and the fine-grained samples consist of semiconducting grains and insulating grain boundaries that primarily lead to an internal barrier layer capacitance (IBLC) effect. And thus, manifest colossal dielectric constant ($\varepsilon_r' > 10^3$) in Eu_2CuO_4 ceramics. The smaller grain size (Pechini) sample, with over an order higher number of grains and grain boundary network, showing over an order higher ε_r' ($\sim 10^5$) compared to the coarse grained one, further endorses the IBLC effect.

Keywords: A. Powders: chemical preparation; B. Grain size; C. Dielectric properties

1. Introduction

Traditionally, ferroelectric materials with high dielectric permittivity (ε_r') have been widely used in capacitive elements in microelectronic circuits. A few of the widely studied ferroelectric materials with high $\varepsilon_r' \geq 10^3$ ($f \leq 10$ MHz) include $BaTiO_3$ [1] and $PbTiO_3$ [2]. These displacive type ferroelectric (FE) materials of non-centrosymmetric, Perovskite structure can be categorized as the intrinsic high ε_r' materials. However, there exists another class of dielectric materials like $CaCu_3Ti_4O_{12}$ (CCTO) [3], $Bi_{2/3}Cu_3Ti_4O_{12}$ [4], which have shown colossal dielectric constant (CDC), $\varepsilon_r' > 10^3$ ($f < 1$ MHz) in spite of being non-ferroelectric (NFE). The origin of such CDC in NFE materials have always been debated, where origin of CDC have been invariably attributed to intrinsic as well as extrinsic property of the material, making its origin uncertain. Amongst the NFEs, CCTO is probably the most widely studied material in this regard and it is widely accepted that the origin of CDC is essentially extrinsic in nature [5–11]. The high ε_r' observed in CCTO, which was initially ascribed primarily to the extrinsic effects caused by polarization of grain boundaries (Maxwell–Wagner effect) and sample-electrode interface [8], was later suggested to be due to the barrier layer capacitance by Subramanian et al. [4]. This notion was subsequently asserted by Sinclair, Adams and West [5–7] based on their impedance spectroscopic studies of polycrystalline CCTO samples, manifesting semiconducting grains and insulating grain boundaries. Further, they established that the Internal Barrier Layer Capacitance (IBLC) [12–13] arising from the grain boundaries was primarily responsible for the high ε_r' in CCTO. The microstructure dependence of grain and grain boundary resistances, probed by impedance spectroscopy (IS) [9,14], and the electrical heterogeneity probed using conducting atomic force microscopy [11] have lent strong support to the IBLC effect being responsible for the high ε_r' in CCTO.

*Corresponding author. Tel.: +91 22 25764621; fax: +91 22 25726975.
E-mail addresses: psalame@iitb.ac.in (P. Salame), ajit.kulkarni@iitb.ac.in, ajit2957@gmail.com (A.R. Kulkarni).

0272-8842/$ - see front matter © 2013 Elsevier Ltd and Techna Group S.r.l. All rights reserved.
http://dx.doi.org/10.1016/j.ceramint.2013.08.123

Apart from the above NFE high ε_r' materials, in the recent past, a few of the pristine layered cuprates *viz*. La_2CuO_4 and Nd_2CuO_4 with T- and T′-type structures respectively [15], have also been reported to show extremely high ε_r' values ($>10^3$, $f \leq 1$ MHz) [16–18]. Thus, the family of pristine cuprates, per se, presents an interesting category of materials to be explored fully for their dielectric properties. Among the Ln_2CuO_4 (Ln=lanthanide) layered cuprates, only the T-type La_2CuO_4 has been investigated in considerable detail for its electrical properties [19–22]. Whereas, amongst the T′-type Ln_2CuO_4 (Ln=Pr, Nd, Sm, Eu, and Gd), only a few selective compositions *viz*. Nd_2CuO_4 [17], Gd_2CuO_4 [18,23] have been studied. The colossal $\varepsilon_r' > 10^3$ ($T < 300$ K, $f < 1$ MHz) reported in Nd- and Gd-cuprates has been hitherto attributed primarily to the intrinsic dipolar effect [17,18], and, in spite of being non-ferroelectric, the possible extrinsic contributions leading to high ε_r' have been hardly accounted for. Thus, it is viewed that a detailed impedance study is needed for asserting the sources of high ε_r' in T′-type cuprates. Recently, on Pr_2CuO_4 ceramic samples we made electrical measurements and IS studies; it has been inferred, based on the finding of insulating grain boundaries and semiconducting grains, that IBLC effect could be dominantly responsible for the occurrence of extremely high $\varepsilon_r' \geq 10^3$ ($-100 < T < 150$ °C, $f \leq 1$ MHz) in Pr_2CuO_4 [24]. In order to enrich the existing sparse electrical data on the T′-type family of cuprates, and to make a definitive assertion of the contribution of extrinsic effects, especially IBLC effect to colossal ε_r', we have fabricated phase pure Eu_2CuO_4 ceramic disk samples of markedly different grain sizes for the dielectric studies. The earlier reported data on the electrical properties of Eu_2CuO_4 compound have been very modest [25,26]. The electrical measurements by Babinskiĭ et al. [25] on a platelet of single crystal Eu_2CuO_4, along the *c*-axis perpendicular to the (*a*–*b*) plane, have shown astonishingly low values of $\varepsilon_r' < 40$ ($T \leq 300$ K, 70 Hz $\leq f \leq 1$ MHz) and very low electrical conductivity, $\sigma = 10^{-9}$ S cm^{-1}. On the other hand, single crystals of La_2CuO_4 (T-type) have shown much larger $\varepsilon_r' \geq 10^3$ ($T \leq 350$ K, $f \leq 1$ MHz) along the *c*-axis, and $\varepsilon_r' > 10^2$–10^3 ($T > 230$ K, $f < 1$ MHz) along the *a*-axis, while $\sigma_c \sim 10^{-4}$ S cm^{-1} and $\sigma_{a-b} \sim 10^{-3}$ S cm^{-1} [21,27,28]. $\varepsilon_r' > 10^4$ ($T > 150$ K) has also been reported in polycrystalline La_2CuO_4 [22]. In view of these observations, dielectric studies on the polycrystalline Eu_2CuO_4 ceramics, hitherto unreported, should be of great merit to explore the possibility of IBLC effect contributing to ε_r' in the T′ layered cuprate.

In this paper, we do report our findings of extremely high dielectric constant ($\varepsilon_r' > 10^3$, $f \leq 1$ MHz) in the ceramic Eu_2CuO_4 disks, synthesized by the conventional powder mixing, solid state reaction and sintering route, giving rise to coarse bar-like grains and grain boundary interfaces. Further still, in order to assess the effect of higher population density of grain boundaries on ε_r', we have prepared fine grained Eu_2CuO_4 ceramic following a wet chemical citrate-complexation Pechini process. This process has facilitated molecular level mixing of the constituent elements; a subsequent careful and relatively low temperature thermal treatment has led to formation of nano-sized T′-phase powder, which could be well sintered at relatively lower temperature. In this sample $\varepsilon_r' \sim 10^5$ ($f \leq 1$ MHz) is obtained, thus, implicating possible IBLC effect to be operative in both, the conventional and the Pechini processed Eu_2CuO_4 ceramics. The analysis of the impedance spectroscopic (IS) data on these samples is also presented here.

2. Experimental details

Polycrystalline nominal Eu_2CuO_4 (T′-phase) samples (in ~20 g batch size) were prepared by conventional powder mixing and ceramic solid state reaction route, as described elsewhere [24]. The phase purity of samples prepared by this method was ensured by matching the recorded powder X-ray diffraction (XRD) pattern of the samples with that of the standard JCPDS data of Eu_2CuO_4. The particle size of the SS reacted, phase formed, and reground powder was determined using laser particle size analyzer (*viz*. Beckman Coulter LS 13320); the mean volume particle size, through optimum grinding, was restricted to ~1 μm. The fine Eu_2CuO_4 phase powder after uniaxial compaction at ~100 MPa in thin disks form was sintered in air at 1100 °C for ~12 h. Also Eu_2CuO_4 sintered disks were fabricated, using fine crystallite size phase formed powder following the citrate complexation Pechini process [29]. For this, the high purity (>99.9%) Eu_2O_3 and CuO in stoichiometric proportions were dissolved in the warm (70 °C) dilute HNO_3 just in sufficient quantity. In the nitrate precursor solution, excess amounts of citric acid (dissolved in water) and ethylene glycol were added. The pH of the solution was maintained strictly at 6.2 by controlled addition of ammonia during the low temperature (~80 °C) thermal drying process. The further heating of the viscous solution to ~120 °C led to the formation of dark navy blue colored gel. The pyrolytic decomposition of the nearly dried gel was effected between 170 and 300 °C. The resulting fine powder was calcined at 550 °C and subsequently solid state reacted in furnace at 820 °C/6 h to make the desired T′-phase Eu_2CuO_4 powder, which was compacted into disk form and sintered at 1000 °C for 6 h in air. The phase purity of the sintered samples formed by the two different processes was checked by their respective powder XRD patterns. For this, PANalytical X'Pert PRO diffractometer system having incident X-ray wavelength $CuK_\alpha = 1.54056$ Å was used. The particle morphology of the phase formed powder prepared by Pechini process was observed using (JEOL JEM-2100) high resolution transimission electron microscope (HR-TEM). The microstructures of the thermally etched surfaces of Eu_2CuO_4 pellets were examined by scanning electron microscope (SEM), JEOL model no. JSM-7600F. The energy dispersive X-ray (EDX) analysis attachment (OXFORD instruments) of SEM was utilized for checking the relative concentrations of the constituent elements present in the grain and the grain boundary regions of the sample. Surface characterization *viz*. X-ray photoelectron spectroscopy (XPS) for verifying the Cu valence state in the sample was carried out using Thermo VG Scientific Multilab 2000 having ESCA probe with AlK_α as X-ray source. For measuring dielectric properties of the sample, the disk

shaped pellets of ~2 mm thickness and ~10 mm diameter were fabricated into parallel plate capacitors by forming metallic electrodes with silver paint, and Novocontrol Alpha A-analyzer with BDS 1200 was used as sample holder. The measurements were carried out in the frequency range 0.1 Hz $\leq f \leq$ 1 MHz at different set temperatures between −100 °C and 150 °C, employing a recording step of 10 °C. All the recorded IS data were corrected for the sample geometry, further, these IS data were analyzed using WinFit and EIS spectrum analyzer software.

3. Results and discussion

3.1. T′-type phase formation and particle size distribution

Fig. 1(a) shows the room temperature powder XRD patterns of the nominal Eu_2CuO_4 ceramic sintered samples synthesized by (i) conventional powder mixing process, and (ii) wet chemical citrate gel complexation (Pechini) process. For both the samples the XRD peaks match well with the T′-phase peaks given in the JCPDS file no. 00-022-0234 (sp. gp. I4/mmm), thus showing phase purity of the samples. For both the samples, the Rietveld refined lattice parameters, using X'Pert Highscore Plus software, are given in Table 1. The measured apparent physical densities of the sintered samples are also listed in Table 1. The inset in Fig. 1(a) shows the particle size distribution histogram of the Eu_2CuO_4 phase formed powder, synthesized by conventional powder mixing. The mean volume particle size is ~1 μm. The TEM images (Fig. 1(b) and (c)) of the particles of Eu_2CuO_4 phase powder, formed by Pechini process, reveal the particles to be consisting of agglomerated crystallites; Fig. 1(b) shows hard agglomerated particle ~100 nm while Fig. 1(c) shows a few weakly agglomerated nearly dispersed crystallites. Further, HR-TEM image (Fig. 1(d)), for the two partly overlapping crystallites, shows the spacings between the lattice planes of (200), and (103), those match well with the $d_{(200)}$ (1.9519(±3) Å) and $d_{(103)}$ (2.7843(±5) Å) spacings obtained from the XRD data.

3.2. Microstructure and EDX analysis

Representative photomicrographs of the thermally etched polished-surfaces of Eu_2CuO_4 pellets prepared by the conventional powder mixing and the Pechini process are, respectively, shown in Fig. 2(a) and (b). Both the photomicrographs show clean grains and fairly dense microstructures. Further, the powder route ceramic sample shows characteristic bar-like grains of varying lengths between 13 and 20 μm, and fairly uniform width between 5.5 and 7 μm, while the Pechini processed sample shows comparatively much smaller grain size albeit having bimodal distribution with average sizes of ~1 and 3 μm (see Table 1). Further, the EDX analysis (Fig. 3) of both the samples (semi-quantitative only, as standard reference was not used), shows a fairly stoichiometric distribution of Eu, Cu, O elements corresponding to the Eu_2CuO_4 phase.

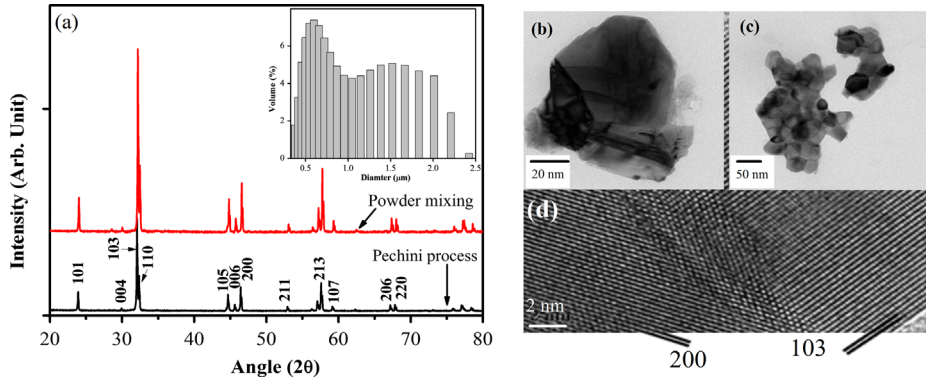

Fig. 1. (a) Powder XRD patterns of T′-type sintered Eu_2CuO_4 samples prepared by (i) conventional powder mixing, and final sintering at 1100 °C for 12 h, post-annealed at 850 °C in oxygen ambience and slow furnace cooled, and (ii) citrate complexation Pechini process, final sintering at 1000 °C for 6 h in air and slow cooled. Inset of (a) shows the particle size distribution of phase formed powder by conventional powder mixing process. The TEM images (b) and (c) of the particles of Eu_2CuO_4 powder, formed by Pechini process, reveal agglomerated crystallites; two partly overlapping crystallites show in (d) the spacings between the lattice planes of (200), and (103), which match well with the $d_{(200)}$ (1.9519(±3) Å) and $d_{(103)}$ (2.7843(±5) Å) spacings obtained from the XRD data.

Table 1
The Rietveld refined lattice parameters computed from the powder XRD patterns of Eu_2CuO_4 (T′-type, sp. gp. I4/mmm) ceramic samples, prepared by two different methods are given here. The average crystallite sizes estimated from the SEM photomicrographs, and apparent sintered densities are also given.

Synthesis method	$a=b$ (Å)	c (Å)	Sintered density	Grain size (see Fig. 2)
Powder mixing	3.901(2)	11.901(5)	96(±0.5) (%TD)	Bar-like ($D^2 \sim 17 \times 7$ μm^2)
Pechini process	3.905(3)	11.902(7)	92.5(±0.3) (%TD)	Bimodal ($D_1 \sim 1$ μm, $D_2 \sim 3$ μm)

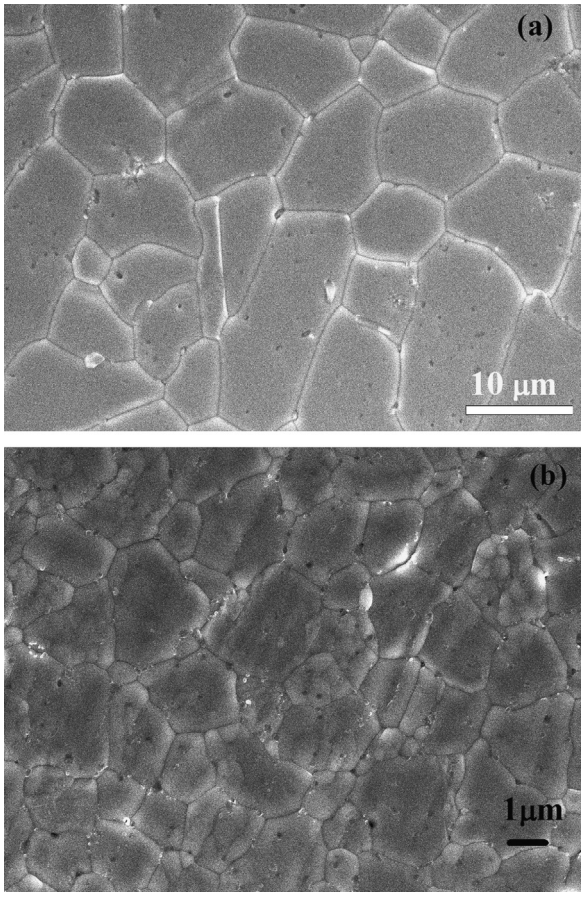

Fig. 2. SEM photomicrographs of the thermally etched polished-surfaces of the Eu_2CuO_4 pellets prepared by (a) conventional powder mixing process, revealing coarse bar-like grains, and (b) Pechini process, showing fine grains with bimodal size distribution.

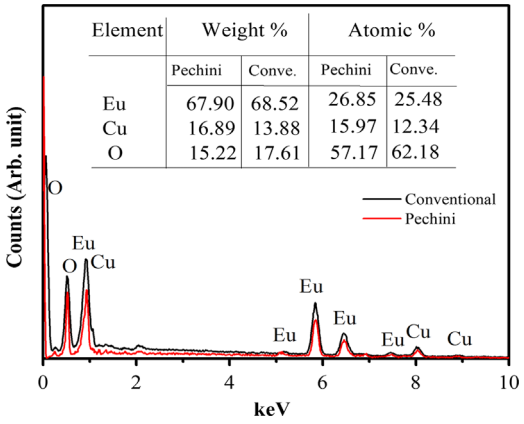

Fig. 3. EDX of the samples prepared by conventional powder mixing, and Pechini process; on analyses, show fairly stoichiometric distribution of Eu, Cu, O elements corresponding to Eu_2CuO_4. Table inside the figure shows the atomic% and weight% distribution of the elements in the sample.

3.3. Cu 2p core-level photoelectron spectra of ceramic Eu_2CuO_4

In Eu_2CuO_4, at high sintering temperatures ($>1000\ ^\circ C$) there is always a possibility of some oxygen loss in the sample and thereby a change in the valence state of a few Cu ions

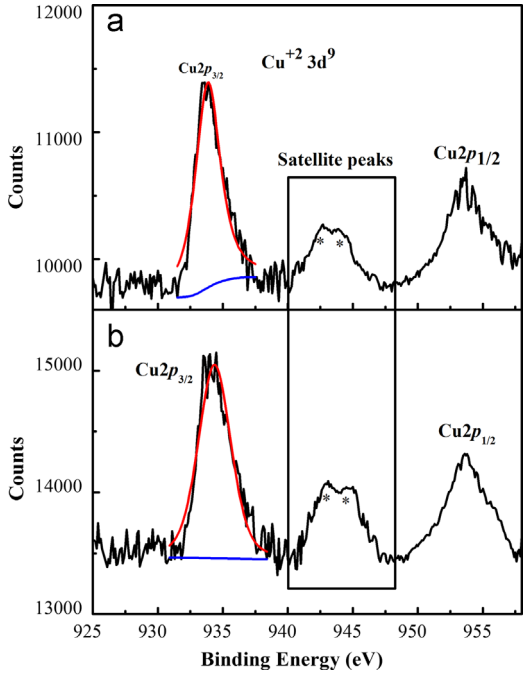

Fig. 4. XPS spectra of Cu 2*p* core level of Eu_2CuO_4 samples prepared by (a) conventional powder mixing process, and (b) Pechini process, revealing +2 ($3d^9$) valence state of Cu in both the samples.

from +2 to +1; X-ray photoelectron spectroscopy (XPS) is a powerful technique to determine the coexistence of Cu^{+2} and Cu^{+1} charge states in a sample. The binding energy spectra corresponding to Cu 2*p* level of Eu_2CuO_4 samples, prepared by the two methods, are shown in Fig. 4. The Cu $2p_{3/2}$ and Cu $2p_{1/2}$ spectra are seen at 933.48 eV and 953.246 eV, and also a satellite peak 9 eV higher in binding energy to that of Cu $2p_{3/2}$ peak. Such a binding energy profile is characteristic of Cu^{+2} (Cu3O bonding) state only [30–32], and, thus, there is no signature of Cu^{+1} in the samples prepared either by the conventional or the Pechini process.

3.4. Dielectric properties

A high value of ε_r' for the polycrystalline coarse grained Eu_2CuO_4 cramic is found from capacitance measurements. The real part of dielectric constant (ε_r') versus frequency (*f*) plots over $10^{-1} \le f \le 10^6$ Hz, for a set of sample temperatures ($-100 \le T \le 150\ ^\circ C$), are shown in Fig. 5. The values of ε_r' reach up the orders of 10^4–10^5, and show a platue in $\varepsilon_r' \sim 5 \times 10^3$ for most of the frequency and temperature ranges. However, with increasing frequency, 10 kHz $< f <$ 1 MHz, ε_r' (see inset of Fig. 5 (a)) falls dramatically for $T \le 0\ ^\circ C$. This type of response of ε_r' with frequency is similar to that observed in other NFE high ε_r' materials, such as CCTO [3–5]. The large contribution to ε_r' below 100 Hz in the samples at $T \ge 50\ ^\circ C$ appears mostly non-intrinsic in nature, and arises mostly due to space charge polarization and/or accumulation of charges at electrodes and at grain boundaries in a polycrystalline sample [8]. Further, the observed sudden drop in ε_r' (Fig. 5(a)) is not accompanied by a corresponding ε_r'' peak (see Fig. 5(b)). Nevertheless, a change in the slope of ε_r'' with *f* is invariably observed, revealing that the

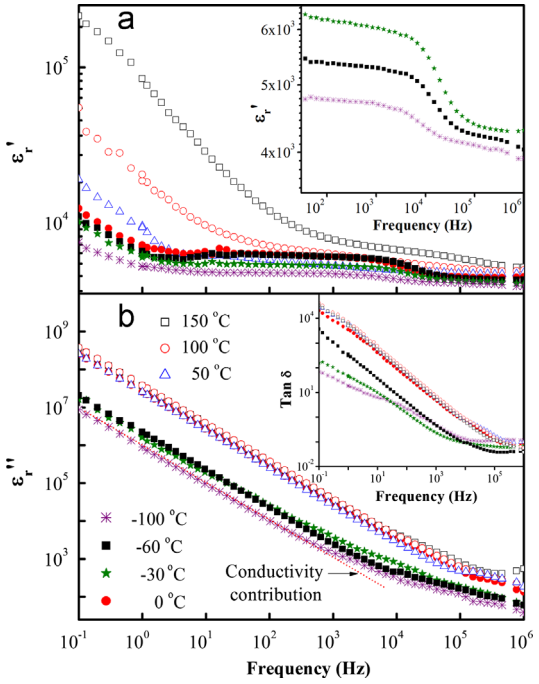

Fig. 5. Frequency dependent response of dielectric parameters of Eu_2CuO_4 coarse grained ceramic at discrete temperatures: (a) real part of the dielectric constant (ε_r'), inset shows the low temperature (≤ -30 °C) data revealing relaxation steps being shifting towards higher frequency with the increase in temperature; (b) imaginary part of the dielectric constant (ε_r''), the inset shows the data for loss factor, tan δ ($\varepsilon_r''/\varepsilon_r'$). The symbols for the curves corresponding to different temperatures in (a), (b), and the inset of (b) are the same.

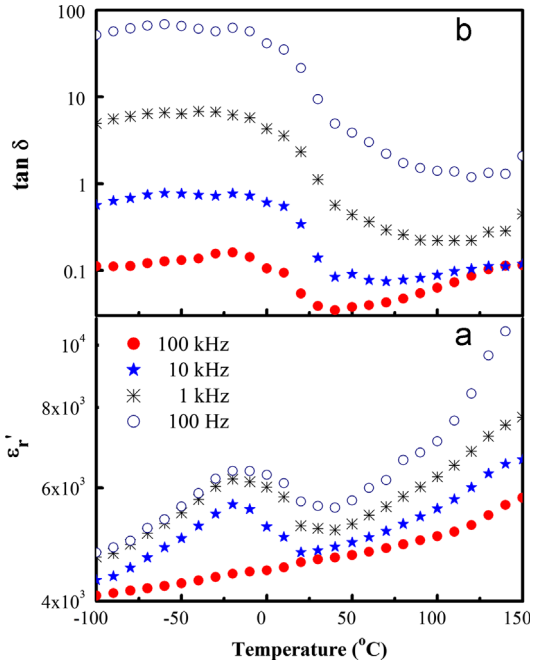

Fig. 6. Temperature dependence of (a) ε_r' and (b) tan δ, at discrete frequencies, for the Eu_2CuO_4 coarse grained ceramic.

relaxation process is not an ideal Debye type. Furthermore, here a slope (log $\Delta\varepsilon_r''$/log Δf) of -1 manifests that electrical conductivity ought to be a contributor to dielectric dissipation (ε_r'') [22,23]. The dissipation in dielectric permittivity can also be seen to follow the equation [33],

$$\varepsilon_r'' \approx (\sigma_{dc}/\varepsilon_o\omega) \quad (1)$$

where, σ_{dc} is conductivity at the lowest measured frequency, ε_o (8.85×10^{-12} Fm^{-1}) is the permittivity of the free space and ω (angular frequency)$=2\nu\pi$. Following this, ε_r'' at high temperatures and low frequencies can be seen increasing, primarily due to the increase in dc conductivity of the sample. The loss factor (tan $\delta=\varepsilon_r''/\varepsilon_r'$) also varies nearly in the same manner as ε_r'' (see inset of Fig. 5(b)) and decreases monotonically with frequency (f), with a slope (log Δtan δ/log Δf) of ~ -1 for $f \leq 10^5$ Hz. From Fig. 5((b) and its inset), it can be easily made out that Eu_2CuO_4 ceramic is electrically quite lossy, with value of ε_r'' reaching $\sim 10^7$–10^8 for 0.1 Hz $\leq f \leq$ 100 Hz, while the tan δ values are between 10 and 10^4 for the same frequency range, and seen increasing with increasing temperature. However, for $f > 10$ KHz, ε_r'' and tan δ show significant drop in their values, especially the tan δ (< 0.1 for 1 MHz).

The temperature (T) dependent dielectric response of the coarse bar-like grained Eu_2CuO_4 ceramic sample is shown in Fig. 6. Exceptionally high values of ε_r' ($> 10^3$) are obtained, for a wide temperature range and over a set of frequencies (see Fig. 6(a)). Further, ε_r' values are nearly temperature independent at $f > 10$ kHz, as compared to those of at lower frequencies ($f \leq 10$ kHz), while tan δ is in the range of 1–0.1 for $f > 10$ kHz. Further, corresponding to a peak in ε_r' at ~ -20 °C, a fall in tan δ value is seen in the proximity of this temperature (see Fig. 6(b)), which is close to the antiferromagnetic ordering temperature ($T_N \sim -8$ °C) of Eu_2CuO_4 material wherein $Cu^{2+}(3d^9)$ ion moments in CuO_2 planes align antiferromgnetically [34,35].

So far, the results show that for $100 \leq f \leq 1$ MHz, the ε_r' values lie between 10^3 and 10^4 for the entire measured temperature range (-100 °C to 150 °C), and ε_r' is seen increasing with increasing temperature but decreases with increasing frequency. The origin of such a large ε_r' ($f > 10$ kHz), cannot be ascribed to the intrinsic character of Eu_2CuO_4 as the work of Babinskiĭ et al. [25] on single crystal platelet of Eu_2CuO_4 has reported $\varepsilon_r' < 40$ (at $f \leq 1$ MHz). Further, the external contribution to ε_r' due to Maxwell–Wagner and other interfacial polarizations are expected to be present only up to few kHz. And although there could be a contribution of conductivity, especially at very low frequencies, as evident from Fig. 5, its contribution at high frequencies diminishes significantly. Therefore, in all probability, it is likely that IBLC effect is operative in Eu_2CuO_4 ceramic and leads to high value of ε_r', as observed in the various NFE materials. In order to further strengthen the prospect of applicability of IBLC effect in Eu_2CuO_4 ceramics, dielectric/impedance studies were also carried out on the fine grained Eu_2CuO_4 ceramic, prepared by Pechini process. It is expected that fine grained microstructure would provide higher density of grain boundary network and, if IBLC effect is operative, should lead to an increase in ε_r'.

The ε_r' dependence on grain size in Eu_2CuO_4 ceramic is evident from Fig. 7(a), wherein a significant upturn in the ε_r'

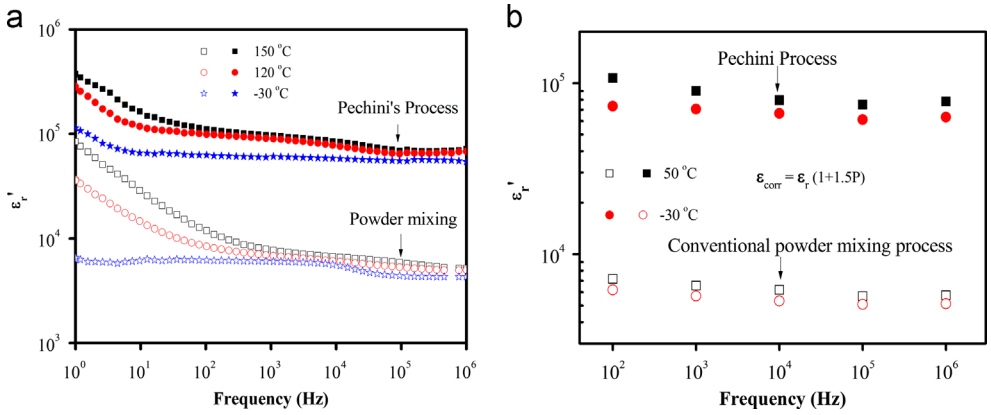

Fig. 7. For the coarse- and the fine-grained Eu_2CuO_4 ceramics: (a) frequency dependence of ε_r', the fine grained sample shows nearly an order higher ε_r' compared to the coarse grained one; and (b) variation of the porsity-corrected ε_r' with frequency at a few select temperatures.

value is seen for the smaller grain size (Pechini) sample. (Since the frequeny and temperature dependent responses of ε_r'' and tan δ of the Pechini processed sample are found to be similar to those obtained for the coarse grained ceramic, hence not repeated here.) Further, as Pechini processed Eu_2CuO_4 pellets show comparatively lower density (92–93% TD) than those of the conventional ones (~96% TD), a porosity corrections to the dielectric values (see Fig. 7(b)) is applied using the porosity correction equation for the single phase ceramics [36,37].

$$\varepsilon_{corr} = \varepsilon_r(1+1.5P), \quad (2)$$

where, ε_r is the observed dielectric constant, and P is the volume fraction porosity of a ceramics. It was interesting to find that in the normalized data, the finer grained ceramics still showed almost an order higher dielectric values. In order to further assert the origin of high ε_r' value, and to establish the presence of IBLC effect leading to such a high ε_r' in Eu_2CuO_4 ceramics, complex impedance plots were analyzed for the samples, and, therby, grain and grain boundary contributions to the overall impedance were calculated.

3.5. Impedance spectroscopy

In Eu_2CuO_4 ceramic, to assess the contribution from grain and grain boundary regions to overall impedance, complex specific impedance plots ($-\rho''=-Z''(A/l)$ versus $\rho'=Z'(A/l)$ (here, A and l are the area and thickness of the sample pellet) for a few selected test temperatures are made (see Fig. 8(a) and (b)) for both the coarse and the fine grained samples. Impedance plots for all the temperatures show semicircles, though the centers of the circles lay somewhat below the real Z axis. Such depressed semicircles essentially represent the distribution of the relaxation times [38]. It is often reported that an ideal Debye like behavior is never obtained in the test samples i.e. the impedance response of a sample cannot be interpreted in terms of simple parallel RC circuit [39,40]. The specific impedance (ρ) plots seen in Fig. 8 for both the samples, having either coarse or fine grains, are not the ideal ones, and deviation from ideal behavior is invariably attributed to contributions arising from grain boundaries, grain orientations and other defects in a ceramic sample. The contributions from each of these entities can be represented by an individual RC circuit. The complex impedance plots Z''–Z' obtained here for Eu_2CuO_4 sample, interestingly, fit more accurately to an equivalent circuit consisting of two parallel RC circuits. The first RC circuit represents the bulk properties of the material, while the second one represents the grain boundaries contribution. The data fitted by the equivalent RC circuits are shown by the continuous curves in Fig. 8. From the RC circuit fittings it is observed that the bulk contribution has lower resistance than the grain boundary contribution. The bulk resistivity (ρ_g) for the coarse as well as fine grained ceramic samples show resistance values of ~1–2 kΩ-cm and is found nearly temperature independent over the entire measured temperature. However, the grain boundary resistivity (ρ_{gb}) is found to be thermally activated, with resistance increasing with decreasing temperature. Further, on calculating the ρ_{gb} values from the plots it is found that $\rho_g \ll \rho_{gb}$, thus showing the samples are electrically heterogeneous with insulating grain boundaries and semiconducting grains. Furthermore, as discussed earlier, as ρ_g values for the Eu_2CuO_4 samples irrespective of grain size are almost equivalent, while the values of ρ_{gb} are up by 1–2 orders of magnitude in the fine grained sample; this shows that the density of grain boundaries in the ceramic dominate the impedance response. Thus it can be inferred, based on the IS studies, that the IBLC effect arising from electrically heterogeneous microstructure is primarily responsible here for high dielectric permittivity. The activation energy of grain boundary conduction (E_{gb}), calculated from the Arrhenius plots (see Fig. 9(a) and inset), for the coarse grained and the fine grained (Pechini) Eu_2CuO_4 ceramics are found to be nearly the same *viz.* 82(1) meV and 80(5) meV respectively for $T > 0$ °C, while for $T < 0$ °C, E_{gb} (33(1) meV) for the coarse grained was found to be higher than that for the fine grained one (E_{gb} ~ 15 meV). The activation energy due to bulk conduction (E_g) in case of fine grained ceramic was 34

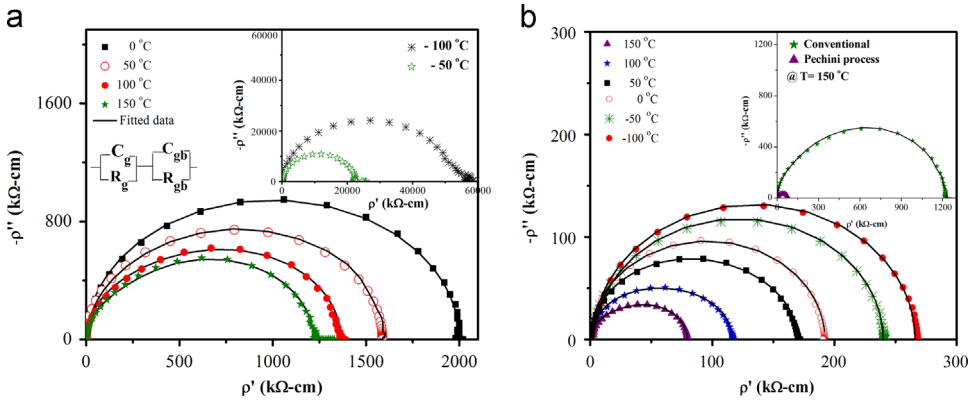

Fig. 8. Specific impedance ($-\rho'' = -Z''(A/l)$ versus $\rho' = Z'(A/l)$ plots at discrete temperatures for a ceramic sample of Eu_2CuO_4 (a) coarse grained and (b) fine grained. The inset of (a) shows the impedance plots for coarse grained sample at high temperatures. The solid lines show the data fitted to the two parallel RC circuits-equivalent model (schematic is shown in the figure). All the data were corrected for the pellet geometry.

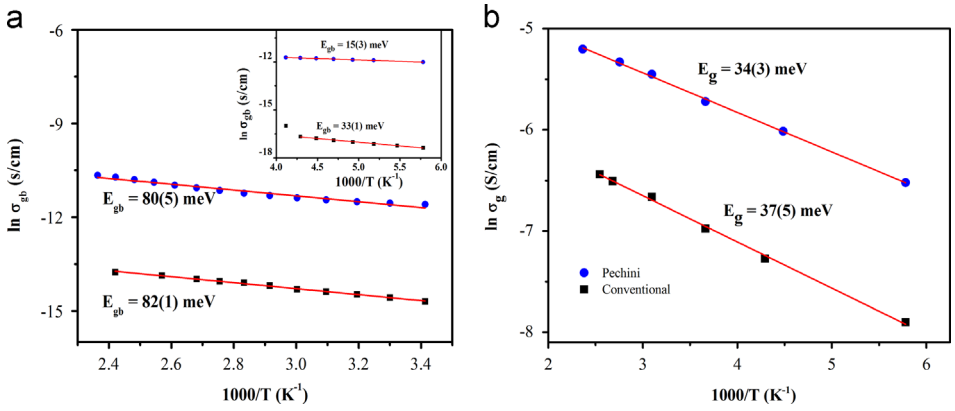

Fig. 9. Activation energy of the grain (E_g) and the grain boundary (E_{gb}) conduction, using Arrhenius plots, of the (a) coarse grained and (b) fine grained Eu_2CuO_4 ceramics.

(3) meV, and 37(5) meV for the coarse grained one, over the entire temperature range, $-100 \le T \le 150$ °C (see Fig. 9(b)).

4. Conclusions

T′-type pristine Eu_2CuO_4 ceramic samples of two markedly different grain sizes were synthesized. Grain size dependent large values of $\varepsilon_r' \sim 10^3$–10^4 (coarse grained) and 10^4–10^5 (fine grained) were observed in the frequency range 1 kHz $\le f \le$ 1 MHz, over the temperatures -100 °C $\le T \le 150$ °C. The IS study of both the coarse- and the fine-grained samples showed them to be electrically heterogeneous with semiconducting grains and insulating grain boundaries, which lent support to the IBLC effect being the primary contributor to ε_r' in the samples. The bulk resistivity (ρ_g) of both the samples had nearly same values; while the grain boundary resistances (ρ_{gb}) differed by 1–2 orders of magnitude, indicating that the grain boundaries dominated the overall impedance, and thus strengthened the assertion that IBLC effect had primarily led to colossal value of ε_r' in the Eu_2CuO_4 ceramics.

Acknowledgments

We acknowledge the IRCC for providing the XPS facility, Mr. Rajan Singh, CRNTS, IIT Bombay for helping in characterizing the samples by SEM and TEM.

References

[1] B.G. Kim, S.M. Cho, T.Y. Kim, H.M. Jang, Giant dielectric permittivity observed in Pb-based perovskite ferroelectrics, Physical Review Letters 86 (2001) 3404–3406.
[2] L.E. Cross, Relaxor ferroelectrics, Ferroelectrics 76 (1987) 241–267.
[3] C.C. Homes, T. Vogt, S.M. Shapiro, S. Wakimoto, A.P. Ramirez, Optical response of high-dielectric-constant perovskite-related oxide, Science 293 (2001) 673–676.
[4] M.A. Subramanian, D. Li, N. Duan, B.A. Reisner, A.W. Sleight, High dielectric constant in $ACu_3Ti_4O_{12}$ and $ACu_3Ti_3FeO_{12}$ phases, Journal of Solid State Chemistry 151 (2000) 323–325.
[5] D.C. Sinclair, T.B. Adams, F.D. Morrison, A.R. West, $CaCu_3Ti_4O_{12}$: one-step internal barrier layer capacitor, Applied Physics Letters 80 (2002) 2153–2155.
[6] T.B. Adams, D.C. Sinclair, A.R. West, Characterization of grain boundary impedance in fine- and coarse-grained $CaCu_3Ti_4O_{12}$ ceramics, Physical Review B 73 (2006) 094124-1–094124-9.
[7] T.B. Adams, D.C. Sinclair, A.R. West, Giant capacitance effects in $CaCu_3Ti_4O_{12}$ ceramics, Advanced Materials 14 (2002) 1321–1323.
[8] P. Lunkenheimer, R. Fichtl, S.G. Ebbinghaus, A. Loidl, Nonintrinsic origin of the colossal dielectric constant in $CaCu_3Ti_4O_{12}$, Physical Review B 70 (2004) 172102-1–172102-4.
[9] T.T. Fang, H.K. Shiau, Mechanism for developing the boundary barrier layer of $CaCu_3Ti_4O_{12}$, Journal of the American Ceramic Society 87 (2004) 2072–2079.
[10] J.L. Zhang, P. Zheng, C.L. Wang, M.L. Zhao, J.C. Li, J.F. Wang, Dielectric dispersion of $CaCu_3Ti_4O_{12}$ ceramics at high temperatures, Applied Physics Letters 87 (2005) 142901-1–142901-3.
[11] D. Fu, H. Taniguchi, T. Taniyama, M. Itoh, S. Koshihara, Origin of giant dielectric response in nonferroelectric $CaCu_3Ti_4O_{12}$: inhomogeneous

conduction nature probed by atomic force microscopy, Chemistry of Materials 20 (2008) 1694–1698.
[12] C.F. Yang, Improvement of the sintering and dielectric characteristics of surface barrier layer capacitor by CuO addition, Japanese Journal of Applied Physics 35 (1996) 1806–1813.
[13] C.F. Yang, An equivalent circuit for CuO modified surface barrier layer capacitors, Japanese Journal of Applied Physics 36 (1997) 188–193.
[14] T.B. Adams, D.C. Sinclair, A.R. West, Influence of processing conditions on the electrical properties of $CaCu_3Ti_4O_{12}$ ceramics, Journal of the American Ceramic Society 89 (2006) 3129–3135.
[15] J.F. Bringley, S.S. Trail, A. Bruce Scott, An ionic model of the crystal chemistry in the superconducting copper oxides of stoichiometry $(RE)_2CuO_4$, Journal of Solid State Chemistry 86 (1990) 310–322.
[16] D. Reagor, E. Ahrens, S.W. Cheong, A. Migliori, Z. Fisk, Large dielectric constant and massive carriers in La_2CuO_4, Physical Review Letters 62 (1989) 2048–2051.
[17] J.W. Chen, J.C. Wang, Y.F. Chen, Study of dielectric relaxation behavior in Nd_2CuO_4, Physica C 289 (1997) 131–136.
[18] J.B. Shi, Y. Hsu, C.T. Lin, Dielectric properties of Gd_2CuO_4, Physica C 299 (1998) 272–278.
[19] P. Lunkenheimer, G. Knebel, A. Pimenov, G.A. Emel'chenko, A. Loidl, DC and AC conductivity of $La_2CuO_{4+\delta}$, Zeitschrift für Physik B 99 (1996) 507–516.
[20] P. Lunkenheimer, M. Resch, A. Loidl, AC conductivity in La_2CuO_4, Physical Review Letters 69 (1992) 498–501.
[21] C.Y. Chen, N.W. Preyer, P.J. Picone, M.A. Kastner, H.P. Jenssen, D. R. Gabbe, A. Cassanho, R.J. Birbeneau, Frequency dependence of the conductivity and dielectric constant of La_2CuO_{4+y} near insulator–metal transition, Physical Review Letters 63 (1989) 2307–2310.
[22] C.C. Wang, Y.M. Cui, G.L. Xie, C.P. Chen, L.W. Zhang, Phase separation in La_2CuO_{4+y} ceramics probed by dielectric measurements, Physical Review B 72 (2005) 0645131–0645136.
[23] J.Y. Mei, H. Wang, G.J. Wang, X.H. Sun, T. Li, C.M. Lei, C.C. Wang, High-temperature dielectric properties of Gd_2CuO_4 ceramics, Physica B 407 (2012) 1082–1085.
[24] P.H. Salame, O. Prakash, A.R. Kulkarni, Extremely high dielectric constant in ceramic Pr_2CuO_4, Journal of the American Ceramic Society 96 (2013) 2184–2189.
[25] A.V. Babinskiĭ, S.L. Ginzburg, E.I. Golovenchits, V.A. Sanina, Orbital glass induced 2D antiferromagnetic fluctuations in Eu_2CuO_4, Pis'ma v Zhurnal Èksperimental'noi i Teoreticheskoi Fiziki 57 (1993) 289–293.
[26] A.M. George, I.K. Gopalakrishnan, M.D. Karkhanavala, Electrical conductivity of Ln_2CuO_4 compounds, Materials Research Bulletin 9 (1974) 721–726.
[27] C.Y. Chen, R.J. Birgeneau, M.A. Kastner, N.W. Preyer, T. Thio, Frequency and magnetic field dependence of dielectric constant and conductivity of La_2CuO_{4+y}, Physical Review B 43 (1991) 392–401.
[28] G. Cao, J.W. O'reilly, J.E. Crow, L.R. Testardi, Enhanced electric polarizability at the magnetic ordering temperature of La_2CuO_{4+x}, Physical Review B 47 (1993) 11510–11511.
[29] M.P. Pechini, N. Adams, Method of Preparing Lead and Alkaline Earth Titanates and Niobates and Coating Method Using the Same to Form a Capacitor, US Patent 3330697, 1967.
[30] J.H. Weaver, H.M. Meyer III, T.J. Wagener, D.M. Hill, Y. Gao, Valence bands, oxygen in planes and chains, and surface changes for single crystals of M_2CuO_4 and $MBa_2Cu_3O_x$ (M=Pr, Nd, Eu, Gd), Physical Review B 38 (1988) 4668–4676.
[31] J. Ghijsen, L.H. Tjeng, J. van Elp, H. Eskes, Electronic structure of Cu_2O and CuO, Physical Review B 38 (1988) 11322–11330.
[32] J. Sugiyama, R. Itti, H. Yamauchi, N. Koshizuka, S. Tanaka, Photoelectron spectroscopy study of superconductive $Nd_2CuO_{4-x}F_x$, Physical Review B 45 (1992) 4952–4956.
[33] S. Maensiri, P. Thongbai, T. Yamwong, Giant dielectric response in (Li, Ti)-doped NiO ceramics synthesized by the polymerized complex method, Acta Materialia 55 (2007) 2851–2861.
[34] T. Chattopadhyay, J.W. Lynn, N. Rosov, T.E. Grigereit, S.N. Barilo, D.I. Zhigunov, Magnetic ordering in Eu_2CuO_4, Physical Review B 49 (1994) 9944–9948.
[35] R.S. Puche, M. Norton, T.R. White, W.S. Glaunsinger, Magnetic properties of the semiconducting lanthanide cuprates Ln_2CuO_4 and their interpretation: evidence for a new series of planar copper antiferromagnets, Journal of Solid State Chemistry 50 (1983) 281–293.
[36] A.J. Bosman, E.E. Havinga, Temperature dependence of dielectric constants of cubic ionic compounds, Physical Review 129 (1963) 1593–1600.
[37] D. Zhou, H. Wang, X. Yao, L.X. Pang, Microwave dielectric properties of low temperature firing $Bi_2Mo_2O_9$ ceramic, Journal of the American Ceramic Society 91 (2008) 3419–3422.
[38] T.S. John Irvine, D.C. Sinclair, A.R. West, Electroceramics: characterization by impedance spectroscopy, Advanced Materials 2 (1990) 132–138.
[39] A.R. West, D.C. Sinclair, N. Hirose, Characterization of electrical materials, especially ferroelectrics, by impedance spectroscopy, Journal of Electroceramics 1 (1997) 65–71.
[40] D.C. Sinclair, A.R. West, Impedance and modulus spectroscopy of semiconducting $BaTiO_3$ showing positive temperature coefficient of resistance, Journal of Applied Physics 66 (1989) 3850–3856.